Olefin Insertion and Subsequent β-X Elimination from a Pentacoordinate Tantalum Complex. A Density Functional Theory Study

Thomas R. Cundari* and Christopher D. Taylor†

Department of Chemistry, University of Memphis, Memphis, Tennessee 38152

Received May 13, 2003

Olefin insertion and metal−alkyl β-X elimination reaction coordinates are followed with density functional theory for a series of X-substituted olefins, where X may be a halide (F, Cl, Br), an ether (OH, OCH_3), hydrogen, or a methyl group, acting on a tantalum dihydride, $Ta(H)_2(OH)_3$. Close comparison is made to the related experimental $Ta(H)_2(OSi\text{-}^tBu_3)_3$ system. Olefin adducts prior to insertion have not been located using several conformational search techniques. Insertion takes place by two primary modes acting in the equatorial plane: endo, between the two hydrides, and exo, to the side of the hydrides. The exo insertion mode is favored by the charge polarized vinyl halides and ethers, and endo insertion is preferred by ethylene and propylene. The kinetic and thermodynamic data obtained by Strazisar and Wolczanski concurs with the activation barriers and reaction enthalpies calculated for both insertion and elimination. β-X elimination is shown to preclude approximate chain propagation (olefin insertion into $Ta-CH_3$) by an energetic preference of between 19 and 29 kcal/mol for vinyl halides and ethers. The β-Me and β-H elimination barriers are of the same order as chain propagation (∼25 kcal/mol).

Introduction

The extraordinary utility of synthetic polymers in the modern world has excited scientific interest regarding advanced polymer design since their theoretical exposition by Staudinger in the 1920s.[1] The discovery of the so-called Ziegler−Natta (ZN) catalysts (offering an unprecedented ability to exercise significant polymer microstructure control) in 1953 opened a new vista of opportunity for inorganic chemists and provided an industrial impetus to the burgeoning field of organometallics.[2] Since that time, the search for high-yield catalysts with novel stereo- and regiochemical properties has continued, a search that has only increased with recent advances in chemical modeling techniques.[3] Attempts to fully characterize the ZN-catalyzed polymerization process have been obfuscated by the sheer number of species arising from the multiplicity of reactions occurring both at and away from the catalytic core and by the inherent alacrity that makes such systems desirable for industrial usage. Theoretical studies, therefore, have been of primary import, providing a staid backdrop against which polymerization catalysis can be measured and explained.[4]

A typical olefin polymerization scheme is presented in Scheme 1. The optimal synthetic pathway involves activation of the catalyst, followed by olefin approach/coordination and subsequent migratory insertion into the metal−alkyl bond. The last two steps repeat themselves (chain propagation) until the advent of a chain-termination event, which may be induced by some means (for example, addition of H_2) to limit the product's molecular weight. One observes in Scheme 1 two alternative pathways to chain propagation, namely β-H and β-alkyl elimination. Proper catalyst design requires the limiting of such pathways relative to chain propagation, as well as the incorporation of correct regio- and stereochemistries for the desired polymer microstructure.

One particular side reaction, β-X elimination, becomes prevalent when the olefin substrate possesses substituents with significant nucleophilic character. Such a functionalization of the substrate leads to the possibility of direct interaction between the substituent and the metal center, at the expense of the metal−olefin interactions critical for chain propagation. That this interaction can pose an obstacle to chain propagation is exemplified in the attempted polymerization of vinyl chloride via a zirconocene catalyst reported by Jordan and Stockland.[5] Rather than obtaining a detectable amount of $(CH_2CHCl)_n$, a plethora of L_nZr-Cl species were produced along with oligopropylene. A β-Cl elimination mechanism was proposed to account for this effect, in which the vinyl chloride is thought to have inserted a la Cossee,[6] followed by rapid β-Cl elimination

* To whom correspondence should be addressed. Present address: Chemistry Department, University of North Texas, Box 305070, Denton, TX 76203.
† Present address: Engineering Physics, University of Virginia, P.O. Box 400238, Charlottesville, VA 22904-4238.

(1) Billmeyer, J., F. W. *Textbook of Polymer Science*, 2nd ed.; Wiley-Interscience: New York, 1971.
(2) Bhaduri, S.; Mukesh, D. *Homogeneous Catalysis: Mechanisms and Industrial Applications*; Wiley-Interscience: New York, 2000.
(3) Casewit, C. J.; Rappe, A. K.; Skiff, W. M. *Chem. Rev.* **2000**, *100*, 1435−1456.
(4) Zamaraev, K. I. *Pure Appl. Chem.* **1997**, *69*, 865−876.
(5) Jordan, R. F.; Stockland, R. A., Jr. *J. Am. Chem. Soc.* **2000**, *122*, 6315−6316.
(6) Cossee, P. *J. Catal.* **1964**, *3*, 80−88.

10.1021/om0303606 CCC: $25.00
Publication on Web 08/26/2003

Scheme 1

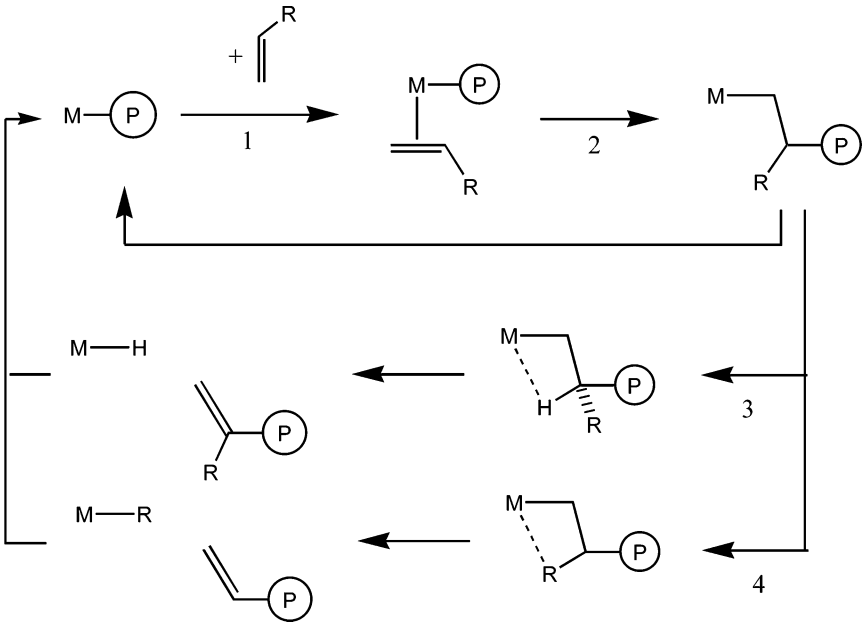

Scheme 2

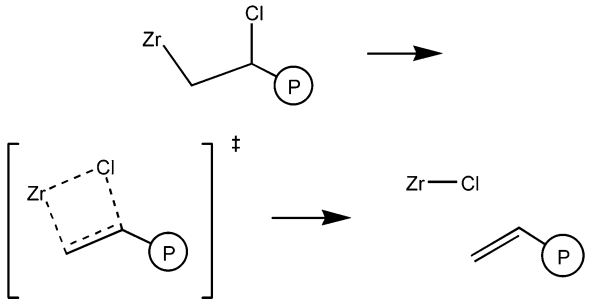

(the microscopic reverse of ethylene insertion into a Zr−Cl bond, Scheme 2).

It is suspected that such a reaction will contribute to a similar inability to synthesize polymers of the form $(CH_2CHX)_n$ directly from olefins of the type $CH_2{=}CHX$ via conventional ZN catalysis. This hypothesis was investigated experimentally by Strazisar and Wolczanski (SW[7]), through the employment of a $Ta(H)_2(OSi\text{-}^tBu_3)_3$ pseudo-catalyst that undergoes insertion and β-X elimination for a series of vinyl halides ($CH_2{=}CHX$) and ethers ($CH_2{=}CHOR$). For both systems (vinyl halides and ethers), β-X elimination was observed to occur to the exclusion of chain propagation. In either case the elimination is kinetically and thermodynamically formidable, with low barriers of activation and significant exothermicity. The solution to the β-X elimination problem therefore requires a theoretically ingenious de novo catalyst design. The insight provided by the SW study serves as a point of departure for elucidating the β-X elimination process via theoretical means.

Despite the increasingly sophisticated theoretical techniques being made available to the chemical world,[8−13] there remains an air of mystery regarding polymerization catalysis and the arena of organometallic chemistry as a whole. The precocity of transition-metal electronics, steric direction, solution phenomena, counterion effects,[12] and ligand spheres[13] together make the elucidation of transition-metal-mediated synthesis a thorny problem indeed. The Cossee−Arlman mechanism[14] of 1964 has proven remarkably robust and served as the framework for all following studies of catalysis to this day.

Computational studies regarding polymerization catalysis to date have principally focused on the critical mechanisms of olefin binding and migratory insertion for simple olefins such as propylene and ethylene.[12,13,16−25] The thesis put forth by Hoffmann and Thorn,[9] suggesting a synergism between metal−hydride σ-donation into the unoccupied olefin π^* orbital and π-donation into the metal−hydride σ^* bond (Scheme 3), provides considerable insight into this process and has been corroborated using ab initio techniques. Other theoretical studies have indicated the importance of agostic interactions,[26]

(7) Strazisar, S. A.; T., W. P. *J. Am. Chem. Soc.* **2001**, *123*, 4728−4740.
(8) Bray, M. R.; Deeth, R. J.; Paget, V. J. *Prog. React. Kinet.* **1996**, *21*, 169−214.
(9) Hoffmann, R.; Thorn, D. L. *J. Am. Chem. Soc.* **1978**, *100*, 2079−2090.
(10) Hoffmann, R.; Lauher, J. W. *J. Am. Chem. Soc.* **1976**, *98*, 1729−1742.
(11) Hall, M. B.; Niu, S. *Chem. Rev.* **2000**, *100*, 353−405.
(12) Fragala, I. L.; Lanza, G.; Marks, T. J. *J. Am. Chem. Soc.* **1998**, *120*, 8257−8258.
(13) Cavallo, L.; Deng, L.; Margl, P. M.; Woo, T. K.; Ziegler, T. *J. Am. Chem. Soc.* **1997**, *119*, 6177−6186.
(14) Arlman, E. J.; Cossee, P. *J. Catal.* **1964**, *3*, 99−104.
(15) Green, M. L. H.; Ivin, K. J.; Mahtab, R.; Rooney, J. J.; Stewart, C. D. *J. Chem. Soc., Chem. Commun.* **1978**, 604−606.
(16) Blochl, P. E.; Woo, T. K.; Ziegler, T. *J. Phys. Chem. A* **2000**, *104*, 121−129.
(17) Blochl, P. E.; Lohrenz, J. C. W.; Margl, P. M.; Woo, T. K.; Ziegler, T. *J. Am. Chem. Soc.* **1996**, *118*, 13021−13030.
(18) Deng, L.; Margl, P.; Ziegler, T. *J. Am. Chem. Soc.* **1998**, *120*, 5517−5525.
(19) Kawamura-Kuribayashi, H.; Koga, N.; Morokuma, K. *J. Am. Chem. Soc.* **1992**, *114*, 2359−2366.
(20) Jin, W. Q.; Koga, N.; Morokuma, K. *J. Am. Chem. Soc.* **1988**, *110*, 3417−3425.
(21) Siegbahn, P. E. M. *J. Am. Chem. Soc.* **1993**, *115*, 5803−5812.
(22) Koga, N.; Morokuma, K.; Yoshida, T. *Organometallics* **1995**, *14*, 746−758.
(23) Lohrenz, J. C. W.; Woo, T. K.; Ziegler, T. *J. Am. Chem. Soc.* **1995**, *117*, 12793−12800.
(24) Deng, L.; Han, Y.; Ziegler, T. *J. Am. Chem. Soc.* **1997**, *119*, 5939−5945.
(25) Sakai, S. *Int. J. Quantum Chem.* **1997**, *65*, 739−747.

Scheme 3

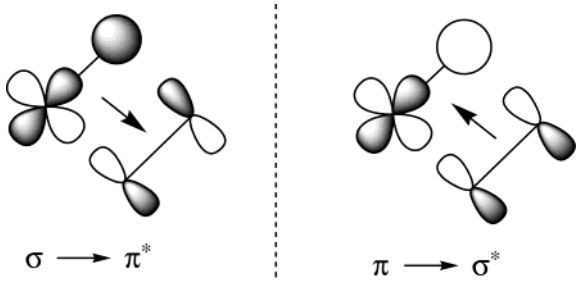

Scheme 4

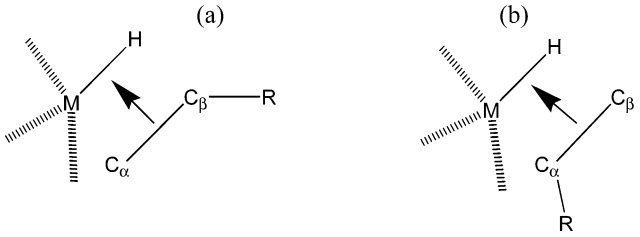

facile rearrangements of the growing chain,[17] and solvent and counterion effects.[12] It is hoped that these insights and more will yield the prized fruit of a superior catalyst design scheme.

Theoretical considerations regarding the heteroatom-substituted olefins are rare. An innovative study by Bercaw et al.[27,28] considered resonance and inductive effects upon the insertion of modified styrenes into transition-metal−hydride bonds. It was found that the transition state was stabilized by π-donating effects and destabilized by electron withdrawal. Steric congestion at C_α dictated a preference for the "linear" (Scheme 4a) versus 'branched' insertion (Scheme 4b). A model for olefin insertion was proposed that involved a zwitterionic transition state (Scheme 5). The developing charge imbalance across the C═C bond on the inserting olefin could be viewed as a cationic C_β, resonance *stabilized* by electron-releasing substituents or *destabilized* by electron-withdrawing effects.

By virtue of their relationship to the insertion procedures, discussions of β-H and β-alkyl elimination often accompany studies of olefin insertion. A density functional theory study of cationic cyclopentadienyl group IX catalysts by Ziegler et al. attributed the higher activation energies required for β-CH_3 elimination to the hindrance resulting from the directionality of the hypothetical methyl lone pair compared to the spherical s orbital active during β-H elimination.[24] On the other hand, calculations on group IV metallocene catalysts by Morokuma et al. suggest that the barriers are relatively the same.[22] Experimentally, β-H elimination is presented as the preferred elimination pathway, with the curious exception of the pentamethylcyclopentadienyl zirconium and hafnium systems of Resconi et al., in which a steric effect between the polymer chain and the ligand sphere is proposed to account for the preferential β-CH_3 elimination from the propyl complex.[29] The logical extension of these reactions to β-X elimination, where X is a heteroatom, remains relatively unstudied, apart from the few cases cited above (Jordan and Stockland, Strazisar and Wolczanski).[5,7]

The work presented herein provides a contribution to the theoretical description of the problem of β-X elimination, by following the experimental work of SW[7] for the analogous system of various vinyl halides and ethers interacting with a $Ta(H)_2(OH)_3$ pseudo-catalyst. The corresponding insertion and β-X elimination reactions proposed by SW are modeled by theoretical means and the electronics rationalized within the Hoffmann donor−acceptor scheme.[9] The determination of the enthalpic reaction profile involving the transient species and transition states associated with these reactions provides an interpretative basis for the kinetics and thermodynamics observed by experiment. Comment is also made regarding the trends in activities of different substrates toward insertion and elimination, with special reference to the competitive effects of chain propagation versus β-X and β-H elimination.

Computational Methods

Energetic modeling and geometry optimization of the various organometallic complexes and transition states was performed using density functional theory (DFT).[30−33] The B3LYP functional was employed for this research; test calculations with other pure and hybrid functionals showed no appreciable dependency.[34] A discussion regarding the competent performance of B3LYP in organometallic modeling can be found in the review by Chermette.[33]

The 6-31G* basis set[35,36] was employed in this work for all main-group atoms and the LANL2DZ effective core potential[37] applied to tantalum, for the reasons of efficiency and inclusion of relativistic effects. Such a combination is denoted LACVP*, following the nomenclature of Titan[38] and Jaguar.[39] Unless otherwise stated, all calculations were performed with Gaussian 98.[40]

To generate initial guess geometries, and to perform conformational searches, Monte Carlo simulations were performed on complexes described by the Merck molecular force field (MMFF)[41] using the molecular operating environment (MOE[42]) software package. Since MMFF has no parameters for tantalum, the geometries of the inner coordination spheres were fixed at crystallographically derived constants for each of the various conformers pursued. The Cambridge Structural Database (CSD[43]) was used for this purpose. Search criteria included organometallic structures without any reported errors, crystallographic disorder, ions or polymeric structures, and $R < 0.05$.

Electronic structure analysis was performed using the natural bond orbital (NBO) theory developed by Reed and Weinhold,[44] provided as a routine within Gaussian 98.

(26) Coates, G. W.; Grubbs, R. H. *Acc. Chem. Res.* **1996**, *29*, 85−93.
(27) Bercaw, J. E.; Burger, B. J.; Santarsiero, B. D.; Trimmer, M. S. *J. Am. Chem. Soc.* **1988**, *110*, 3134−3146.
(28) Bercaw, J. E.; Doherty, N. M. *J. Am. Chem. Soc.* **1985**, *107*, 2670−2682.
(29) Abis, L.; Fiorani, T.; Franciscono, G.; Piemontesi, F.; Resconi, L. *J. Am. Chem. Soc.* **1992**, *114*, 1025−1032.
(30) Holthausen, M. C.; Koch, W. *A Chemist's Guide to Density Functional Theory*; Wiley-VCH: Weinheim, Germany, 2000.
(31) Haque, A.; Kaldor, U. *Chem. Phys. Lett.* **1985**, *120*, 261−265.
(32) Ziegler, T. *Can. J. Chem.* **1995**, *73*, 743−761.
(33) Chermette, H. *Coord. Chem. Rev.* **1998**, *178−180*, 699−721.
(34) Becke, A. D. *J. Chem. Phys.* **1993**, *98*, 5648−5652.
(35) Binning, J., R. C.; Curtiss, L. A. *J. Comput. Chem.* **1990**, *11*, 1206−1216.
(36) Ditchfield, R.; Hehre, W. J.; Pople, J. A. *J. Chem. Phys.* **1972**, *56*, 2257−2261.
(37) Hays, P. J.; Wadt, W. R. *J. Chem. Phys.* **1985**, *82*, 270−283.
(38) *Titan*; Wavefunction, Inc., and Schrodinger, Inc., 1999.
(39) *Jaguar*; Schrodinger, Inc., 1998.
(40) *Gaussian 98*, Revision A.6; Gaussian, Inc., 1998.
(41) Halgren, T. A. *J. Comput. Chem.* **1995**, *17*, 490−519.
(42) *MOE*, version R2000.02; Chemical Computing Group, 2000.
(43) Experimental data were obtained from the Cambridge Structural Database System, using Conquest version 1.3 (Allen, F. H.; Kennard, O. *Chem. Des. Autom. News* **1993**, *8*, 31).

Scheme 5

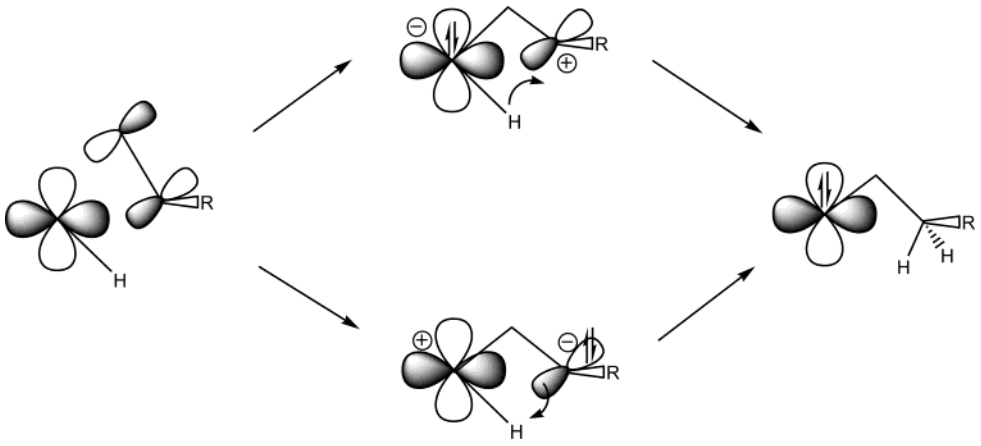

Table 1. Mean ⟨Ta−X⟩, Sample Standard Deviation σ_{Ta-X}, and Sample Size *n* for Ta−X Bond Lengths Extracted from the Cambridge Structural Database (in Å)

	⟨Ta-X⟩	σ_{Ta-X}	n
Ta−H	1.72	0.10	66
Ta−C(sp^3)	2.21	0.05	169
Ta−OR	1.91	0.05	146
Ta−F	1.97	0.16	7
Ta−Cl	2.42	0.08	209
Ta−Br	2.58	0.08	6

Cartesian coordinates of B3LYP/LACVP* optimized stationary points along the olefin insertion and β-X elimination reaction paths are given in the Supporting Information. All species are closed-shell singlets and have been optimized using the restricted Kohn−Sham formalism. The vibrational frequencies were calculated at all stationary points to identify pertinent species as minima (no imaginary frequencies) or transition states (one imaginary frequency).

Results and Discussion

1. Metal−Hydride Complex. The Cambridge Structural Database[43] (CSD) was searched for likely geometric parameters of the model system. Typical Ta−H, Ta−C, Ta−OR, and Ta−X bond lengths were gleaned (Table 1), and trigonal-bipyramidal coordination was suggested. Approximate structural and geometric isomers of the relevant tantalum complexes were constructed accordingly. Cursory molecular mechanics Monte Carlo simulations were conducted in order to search the conformer space, as a result of which both trigonal-bipyramidal and square-pyramidal geometries were considered in the subsequent ab initio study.

B3LYP/LACVP* energies (electronic plus zero point) of the various geometry-optimized isomers (trigonal-bipyramidal and square-pyramidal $Ta(H)_2(OH)_3$) were calculated using Titan. Only two unique minima, *cis*-dihydride trihydroxy square-pyramidal tantalum (Figure 1a) and di-equatorial-hydride trihydroxy trigonal-bipyramidal tantalum (Figure 1b), were found. The latter complex is energetically preferred by 6.9 kcal/mol. The Ta−H distances lie within the 1.7 ± 0.1 Å range of Ta−H bond distances culled from the CSD.

The related (although more sterically encumbered) $Ta(H)_2(OSi^tBu_3)_3$ complex synthesized by LaPointe et al.[45] was reported to have the dis-axial-hydride trihydroxy trigonal-bipyramidal geometry upon interpretation of the powder infrared spectrum (Table 2a). Although this seems plausible from a steric argument, CSD mining indicates that trigonal-bipyramidal tantalum complexes more typically (13 out of 17 unique structures—the remaining 4 contain chelates) have softer ligands disposed equatorially and harder ligands disposed axially (see, for example, refcodes TORXUT, JIHWOM, and JUQZIE[46−48]). This preference was predicted by Rundle[49] and Hoffmann[50] upon the predilection for electron-rich three-center−two-electron bonding about the axial and central sites. Furthermore, no bis-axial minimum was located in directed DFT searches

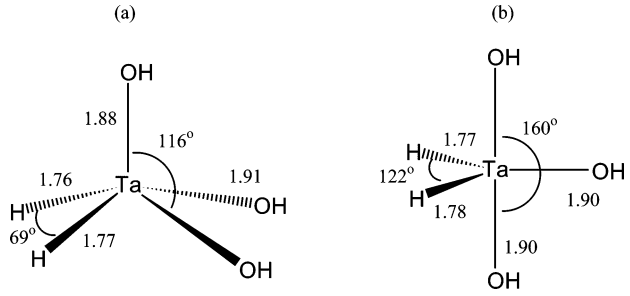

Figure 1. Local minima of $Ta(H)_2(OH)_3$: (a) *cis*-dihydride square pyramidal; (b) di-equatorial-hydride trigonal bipyramidal. Distances are given in Å.

Table 2. Vibrational Modes (given in cm^{-1}) Observed by Experiment[45] and B3LYP/LACVP* Calculation for a Series of $Ta(H)_2(OR)_3$ Model Complexes (This Work)

model	ν(Ta−H/D)	$\delta(TaH_2/D_2)$
(a) Experiment		
$Ta(H)_2(OSi^tBu_3)_3$	1725/1250	750/570
(b) B3LYP/LACVP* Calculation		
$Ta(H)_2(OH)_3$	1756/1249	830/548
$Ta(H)_2(OMe)_3$	1736/1278	786/508
$Ta(H)_2(OSiH_3)_3$	1783/1268	810/587
$Ta(H)_2(OSiMe_3)_3$	1759/1251	795/576

(44) Reed, A. E.; Weinhold, F. *J. Chem. Phys.* **1985**, *83*, 1736−1740.
(45) LaPointe, R. E.; Miller, R. L.; Roe, S. C.; Toreki, R.; Wolczanski, P. T.; Van Duyne, G. D. *J. Am. Chem. Soc.* **1993**, *115*, 5570−5588.
(46) Bruck, M. A.; Fox, P. A.; Gray, S. D.; Wigley, D. E. *Inorg. Chem.* **1996**, *35*, 6027−6036.
(47) Chesnut, R. W.; Fanwick, P. E.; Jacob, G. G.; Rothwell, I. P.; Yu, J. S. *Organometallics* **1991**, *10*, 321−328.
(48) Guzyr, O. I.; Lehmann, C.; Murugavel, R.; Noltemeyer, M.; Roesky, H. W.; Schimkowiak, J.; Schmidt, H.; Schromann, M.; Walawalkar, M. G. *Organometallics* **1999**, *18*, 832−836.
(49) Rundle, R. E. *J. Am. Chem. Soc.* **1963**, *85*, 112−113.
(50) Hoffmann, R.; Rossi, A. R. *Inorg. Chem.* **1975**, *14*, 365−374.

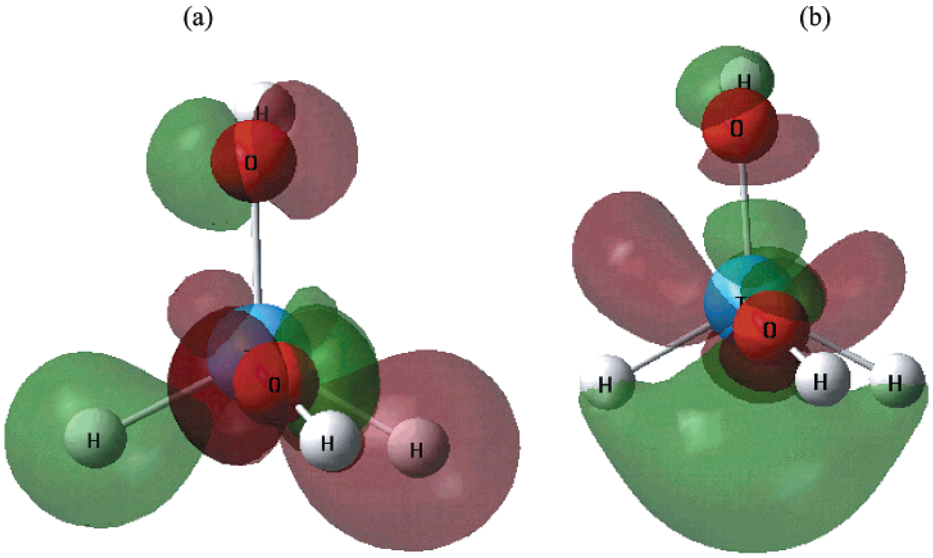

Figure 2. KS-HOMO (a) and KS-LUMO (b) for trigonal-bipyramidal di-equatorial-hydride trihydroxy tantalum.

Scheme 6

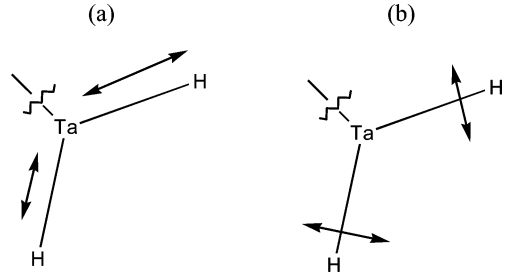

Chart 1

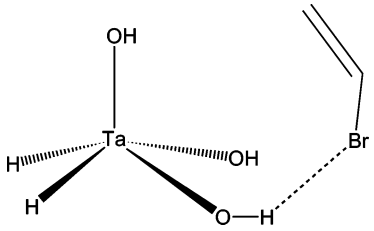

of the conformer space for both −OR and $-OSiR_3$ model ligands (R = H, CH_3). Symmetry-constrained calculations at the bis-axial D_{3h} geometry indicate high-energy structures with imaginary frequencies indicative of instability.

Vibrational mode (ν(Ta−H) and δ(H−Ta−H), Scheme 6) analyses (Table 2b) show consistent agreement with experiment throughout the range of increasingly more "realistic" bis-equatorial systems, suggesting a misassignment of frequencies in the experimental work.

The highest occupied Kohn−Sham molecular orbital (KS-HOMO) for trigonal-bipyramidal $Ta(H)_2(OH)_3$ can be described as a three-center−two-electron $Ta(d_{xy})H(s)$-H(s) bonding orbital between the tantalum and the hydride ligands (Figure 2a). The hydride are somewhat electron donating (contributing 65% of the bond electron density by NBO). An antibonding relationship is noted between the tantalum d_{xy} and the p_x orbital on the oxygen. The Ta−H distances are roughly equal (1.77, 1.78 Å), and the Ta−O distances are all 1.90 ± 0.01 Å, both compatible with surveys of bond distances taken from the CSD (Table 1). The KS-LUMO (lowest unoccupied Kohn−Sham molecular orbital) is primarily antibonding between the $Ta(d_{x^2-y^2})$ and two H(s) orbitals (Figure 2b), with an electronically accessible lobe presented between the hydride ligands (the endo position). It may be anticipated that this will be the site at which π-donation and subsequent insertion occurs.

2. Olefin Adduct. Olefin insertion is typically initiated by formation of a metal−olefin adduct,[11,18,51−54] either through electrostatics or the back-donating Dewar−Chatt−Duncanson model.[55] The diminished electrophilicity of tantalum with respect to typical Ziegler−Natta TMs, and its diminished capacity for back-donation (formally d^0), makes olefin complexation an unlikely step. No such adduct was observed by experiment,[7] although hypothesized by SW. Computational searches for a π-bonded $Ta(CH_2{=}CH_2)(H)_2(OH)_3$ adduct leading to insertion also proved unsuccessful.

An electrostatic adduct apparently irrelevant to the purposes of the present study was observed, however, for the case of X = OH, OCH_3, Br, Cl, F. Close-neighbor interactions between X and the hydroxyl hydrogen of a *square-pyramidal* $Ta(H)_2(OH)_3$ form a weakly bound complex on the order of 4 kcal/mol (Chart 1 illustrates this for X = Br).

3. Insertion Transition State. The deuteration experiments by SW strongly suggest the presence of four-centered transition states governing both insertion and elimination.[7] Activated complexes of this form were constructed using bond distances intermediate to those of the reactant and product, and the geometries were then refined using DFT saddle-point searches. Two types of transition state (TS) were observed, both of which contained the active species within the equatorial plane. The first type corresponds to an exo insertion (Figure 3a), in which the olefin inserts between the migrating hydride ligand and the hydroxy ligand, and

(51) Frenking, G.; Sola, M.; Torrent, M. *Chem. Rev.* **2000**, *100*, 439−493.
(52) Stromberg, S.; Svensson, M.; Zetterberg, K. *Organometallics* **1997**, *16*, 3165−3168.
(53) Yamamoto, A. *J. Chem. Soc., Dalton Trans.* **1999**.
(54) Rooney, J. J.; Webb, G. *J. Catal.* **1964**, *3*, 488−501.
(55) Chatt, J.; Duncanson, L. A. *J. Chem. Soc.* **1952**, *1953*, 2939−2947.

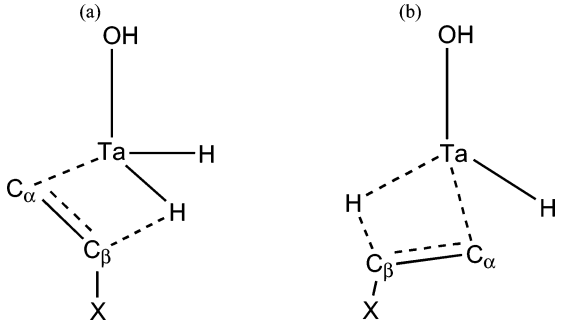

Figure 3. Exo (a) and endo (b) modes for olefin insertion into $Ta(H)_2(OH)_3$. Only the equatorial plane is shown. Note the angular distortion about tantalum in the exo mode.

Table 3. Energetics for Olefin Insertion/β-X Elimination[a]

X	TS	alkyl	X-elim	elim	*P*
F-exo[b]	3.7	−32.8	7.3	−28.0	−60.8
F-endo	7.8	−32.8	13.4	−28.0	−60.8
Cl-exo	6.3	−29.8	6.5	−17.7	−47.6
Cl-endo	10.7	−29.8	13.5	−17.7	−47.6
Br-exo	4.2	−36.1	4.4	−19.7	−55.7
Br-endo	196.9	−36.1	186.3	−19.7	−55.7
OH-exo	1.7	−29.3	17.7	−15.9	−45.3
OH-endo	8.5	−29.3	56.9	−15.9	−45.3
OCH_3-exo	0.0	−30.7	19.0	−13.8	−44.4
OCH_3-endo	nl[c]	−30.7	26.7	−13.8	−44.4
H	10.0	−23.3	33.3	23.3	0.0
H-endo	5.1	−23.3	28.4	23.3	0.0
CH_3-exo	10.6	−18.0	50.0	16.8	−1.2
CH_3-endo	7.2	−18.0	43.1	16.8	−1.2

[a] Energetics (in kcal/mol) are relative to isolated reactants ($Ta(OH)_3(H)_2$ and $H_2C{=}C(H)X$). TS is the olefin insertion barrier for $H_2C{=}C(H)X$ into the Ta−H bond of $Ta(OH)_3(H)_2$, while alkyl is the energy of this insertion to produce an alkyl ($Ta(OH)_3(H)$-(CH_2CH_2X)) complex. X-elim denotes the barrier to β-X elimination from the alkyl, and elim is the energy of the β-X elimination process to produce $Ta(OH)_3(H)(X)$ and ethylene. *P* is the energetics of the overall process $Ta(OH)_3(H)_2 + H_2C{=}C(H)X \rightarrow Ta(OH)_3(H)(X) + H_2C{=}CH_2$). All quoted energies include the zero-point energy correction. [b] Exo and endo refer to the two different regiochemistries of addition; see text for further details. [c] nl = not located. The transition state for endo insertion of methyl vinyl ether into the Ta−H bond of $Ta(OH)_3(H)_2$ could not be isolated, despite numerous attempts from many different starting geometries.

the second to an endo insertion (Figure 3b), in which the olefin inserts between the hydride ligands. The exo TS is preferred for ethylene and propylene insertion (X = H, CH_3) and the endo TS for the insertion of vinyl halides and ethers. Reaction profiles for these reaction mechanisms are summarized in Table 3.

Following the Hoffman model for olefin insertion, olefin π-donation into the LUMO of the tantalum dihydride occurs synchronously with tantalum hydride σ-donation into the olefin π^* orbital. Baerends et al.[56] as well as Stowasser and Hoffmann[57] have discussed the validity of orbital analysis using Kohn−Sham orbitals.

Since the $Ta(H)_2(OH)_3$ LUMO contains a prominent endo-presenting lobe (Figure 2b), one would suggest a greater likelihood for endo insertion upon electronic grounds and indeed one sees a lower barrier to insertion via the endo mode (5.1 and 7.2 kcal/mol), as opposed to the exo mode (10.0 and 10.6 kcal/mol), for the insertions of ethylene and propylene, respectively. This leads to the question of why vinyl halides and ethers preferentially insert via the exo mode. The formation of such a transition state causes a severe distortion of the hydride plane, as demonstrated in Figure 3a. The KS-HOMO and KS-LUMO of this distorted dihydride trihydroxy tantalum species are presented in Figure 4.

Estimates as to the "earliness" or "lateness" of the transition state can best be made by following the C−C bond length, which increases by ∼0.2 Å upon insertion and vice versa upon elimination. It is seen that for the insertion reaction the transition states in all cases (both exo and endo) can be considered early, although the endo TS is slightly more advanced than the exo. For exo insertion of ethylene, the calculated TS is extremely early in nature ($\Delta(C{-}C)_{INS} = 0.01$ Å; 5% advancement)! This result is at best curious and at worst suspect, in that the expectedly similar exo TS for propylene insertion exhibits a geometry closer to that of the inserting heteroatom-substituted olefins than to the ethylene insertion. The exo ethylene TS also exhibits a much lower imaginary vibrational mode (∼30i cm^{-1}, cf. ∼300i cm^{-1} for generic $CH_2{=}CH(X)$). Geometry optimizations from different starting points (altering the $CH_2{=}CH$-(F) insertion and subsequent β-X elimination TS as well as those for $H_2C{=}CH(CH_3)$) were conducted, with no variation occurring in the TS geometry. This potentially interesting result has yet to be rationalized.

As previously mentioned, β-H elimination is the microscopic reverse of olefin insertion, just as chain propagation is the approximate microscopic reverse of β-Me elimination (calculations by Ziegler et al.[18] indicate that insertion into $M{-}CH_2CH_3$ is a better model for chain propagation). It is found that the β-H elimination barrier is 28.4 kcal/mol for a tantalum ethyl complex and 25.2 kcal/mol for a tantalum propyl complex, the difference supposedly arising from the stabilization of the reactant via agostic interactions as discussed below. The chain propagation barrier is 26.3 kcal/mol for ethylene inserting into $Ta(CH_3)(H)(OH)_3$, which is 21.2 kcal/mol higher than the barrier for ethylene insertion into $Ta(H)_2(OH)_3$. This concurs with the observations of Ziegler et al.,[24] who attribute the higher chain propagation barrier to the limited directionality of the trivalent sp^x methyl species, compared to the more electronically accessible s hydride.

Rationalization of substrate preferences for an exo versus endo TS can be made by following an examination of the KS-HOMO and KS-SHOMO (second highest occupied molecular orbital) for each TS. The case of propylene insertion is used as an example. Figure 5 presents B3LYP/LACVP* contour plots for these high-energy orbitals, and the corresponding molecular orbital depictions are given in Figure 6. One can qualitatively describe the exo HOMO as Ta−H σ-donation to olefin π^*. The resultant π/π^* mixing invokes node formation (and therefore charge deficit) at C_β. Similarly, the SHOMO as appears to be olefin π-donation into the LUMO of the tantalum dihydride. Hoffmann's simple σ/σ^* description does not suffice here; the LUMO of the distorted dihydride is a *nonbonding* $Ta(d_{xy})$−H(s) combination rather than an *antibonding* Ta−H σ^*.

(56) Baerends, E. J.; Gritsenko, O. V. *J. Phys. Chem.* **1997**, *101*, 5383−5403.
(57) Stowasser, R.; Hoffmann, R. *J. Am. Chem. Soc.* **1999**, *121*, 3414−3420.

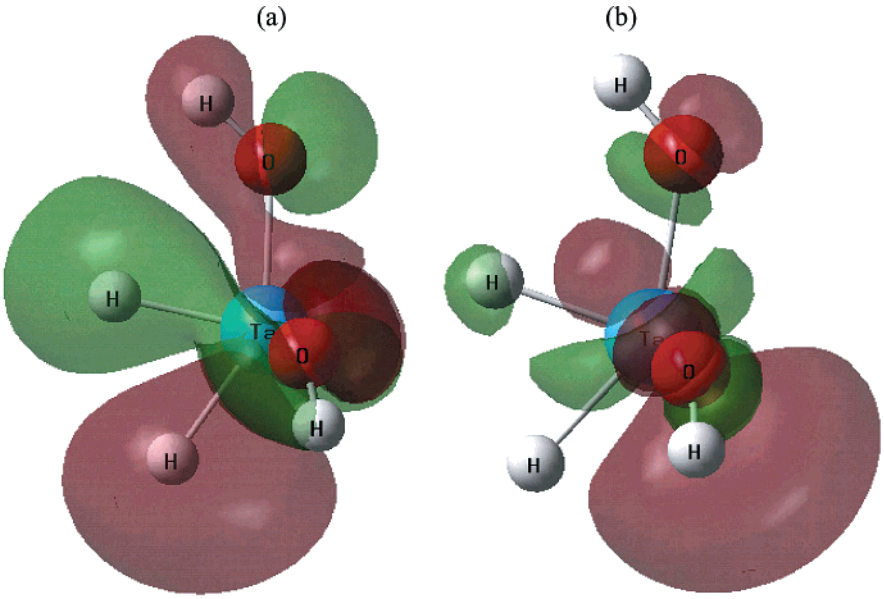

Figure 4. KS-HOMO (a) and KS-LUMO (b) for $Ta(H)_2(OH)_3$ in the exo insertion arrangement.

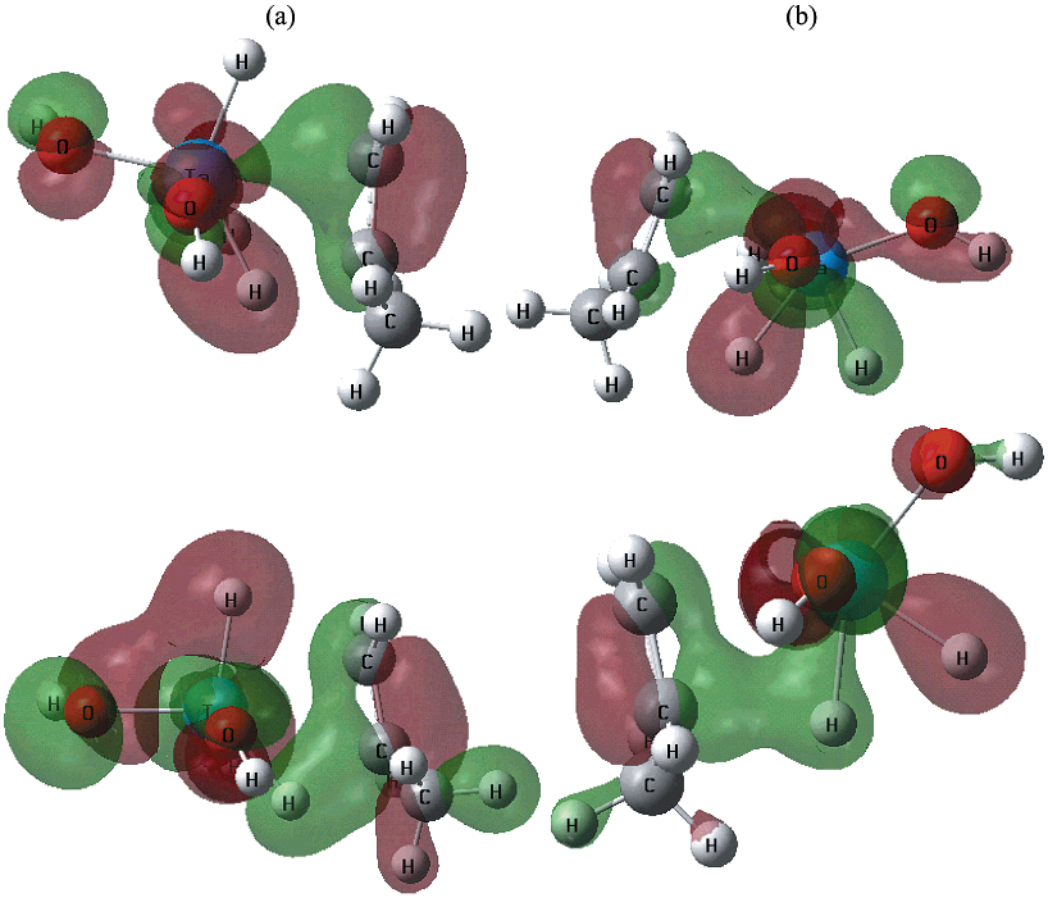

Figure 5. KS-HOMO (top) and KS−SHOMO (bottom) for insertion of propylene into $Ta(H)_2(OH)_3$: (a) endo mode; (b) exo mode.

The HOMO and SHOMO assignments for the endo TS are switched; π-donation is now manifest in the HOMO and σ-donation in the SHOMO. π-Donation is therefore more significant factor for the endo TS. The node at C_α in the endo SHOMO suggests the presence of charge-directing effects between C_α and C_β, reminiscent of the *zwitterionic* picture of olefin insertion presented by Bercaw et al.[28] (Scheme 5).

The electron-withdrawing effects of the substituents in the vinyl halides and ethers diminish the latter's capacity to act as π-donors. It is therefore proposed that the endo TS (in which π-donation is more critical) will be energetically destabilized relative to that for the hydrocarbon olefins, ethylene and propylene. This is indeed the case. On the other hand, the exo TS contains a charge deficit on C_β, one that may be readily stabilized

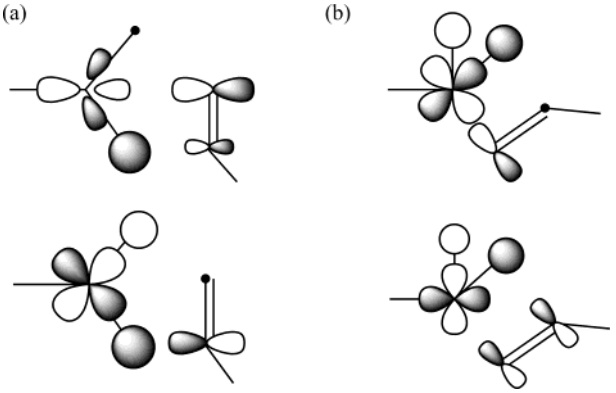

Figure 6. Orbital depictions of the KS-HOMO (top) and KS-SHOMO (bottom) for each of the insertion transition states presented in Figure 5: (a) endo mode; (b) exo mode.

Scheme 7

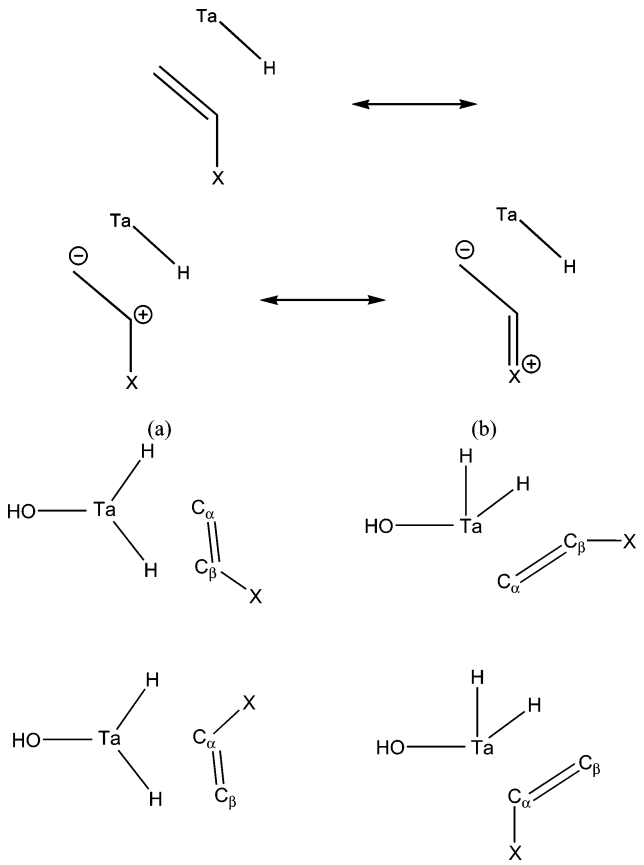

Figure 7. Linear (top) versus branched (bottom) insertion TS: (a) endo mode; (b) exo mode.

by Lewis resonance structures offered by the substituent (Scheme 7). Thus, it is consistent to note that exo insertion barriers are lowest for X = OH, OCH_3, slightly higher for the halides, in the order Cl > Br > F, and greatest for the hydrocarbon olefins ethylene and propylene, a trend borne out precisely in the kinetic measurements of SW.[7]

The preceding arguments also suggest that the charge deficit arising on C_α in the endo insertion would be partially stabilized in a branched endo insertion TS but not in the linear endo insertion TS (Figure 7 compares these two TS for both endo and exo insertion modes). Investigations using vinyl fluoride show that the branched endo insertion (10.1 kcal/mol) is preferred by 2.8 kcal/mol to the branched exo insertion (12.9 kcal/mol), both of which are higher than the linear transition states, for which the exo insertion (3.7 kcal/mol) is more stable than the endo insertion (7.8 kcal/mol) by 4.1 kcal/mol.

Table 4. NBO-Derived Pauling Bond Orders [$n - n^*$]/2 Comprising the Four-Centered Transition States for Insertion and β-X Elimination[a]

(a) Insertion

	Ta−H		Ta−C		C=C		C−H	
	endo	exo	endo	exo	endo	exo	endo	exo
F	0.67	0.71	0.62	0.56	1.68	1.79	0.58	0.41
Cl	0.68	0.71	0.59	0.55	1.69	1.77	0.56	0.41
Br	0.68	0.74	0.58	0.51	1.70	1.81	0.56	0.38
OH	0.64	0.68	0.66	0.62	1.64	1.73	0.61	0.46
OCH_3		0.40		0.64		1.73		0.45
H	0.68	0.90	0.59	0.38	1.71	1.94	0.58	0.25
CH_3	0.67	0.72	0.61	0.53	1.69	1.82	0.58	0.39

(b) β-X Elimination

	Ta-X		Ta−C		C=C		C−X	
	endo	exo	endo	exo	endo	exo	endo	exo
F	0.85	0.85	0.42	0.74	1.71	1.72	0.83	0.84
Cl	0.81	0.85	0.52	0.75	1.59	1.67	0.85	0.81
Br[b]		0.84		0.74		1.66		0.80
OH	0.83	0.88	0.74	0.65	1.71	1.74	0.79	0.79
OCH_3	0.82	0.88	0.72	0.67	1.72	1.74	0.78	0.77
H	0.68	0.89	0.59	0.38	1.71	1.94	0.58	0.25
CH_3	0.64	0.64	0.65	0.66	1.62	1.68	0.73	0.65

[a] Endo and exo forms are given as shown. [b] Endo structures could not be located for these particular transition states.

NBO analysis of the early and late Lewis depictions of the insertion TS signifies that the exo insertion is electronically less developed (i.e., earlier) than the endo insertion; that is to say, Ta−H and C=C Pauling bond orders, $(n(\sigma) - n(\sigma^*))/2$, are higher in the exo TS whereas the Ta−C and C−H bond orders are lower, relative to the endo TS (Table 4). Calculation of natural atomic charges (Table 5) indicate that the olefin inserting via an exo form is electron poor compared to that inserting via an exo form. Conversely, the migrating hydride is electron rich in the exo TS and tantalum is electron poor, again relative to the endo TS.

The charge disparity between C_α and C_β is magnified in the exo TS. As predicted by the molecular orbital description given previously, the charge on C_β is more positive in the exo TS than the endo TS as a consequence of node development in the HOMO. The similarly expected charge diminution at C_α in the endo TS is not observed, perhaps due to the change in predominant insertion modes from olefin π-donation (Scheme 8a) to a charge-transfer description (Scheme 8b).

The seemingly anomalous ordering of exo insertion barriers for the halides (F < Cl < Br) can be rationalized by a combination of charge transfer and π/π^* mixing effects. The HOMO/LUMO gap for CH_2=CHX decreases down the halide group as 177.1, 163.9, and 157.9 kcal/mol, allowing greater π/π^* mixing for the heavier halides and therefore suggesting a swifter insertion. Examination of the natural atomic charges for these substituted ethylenes, however, indicates that the fluoride is more directly withdrawing, the charge on C_β decreasing as 0.47, 0.01, and −0.12 down the group, leading to an expected greater development of C−H bonding in the lighter halides. This is indeed observed (Table 4). An

Table 5. Natural Atomic Charges for the Various CH_2CH_3X Insertion Transition States[a]

	$q(C_\alpha)$		$q(C_\beta)$		$q(C_2H_3X)$		q(H)		q(Ta)	
	exo	endo	exo	endo	exo	endo	exo	endo	exo	endo
H	−0.48	−0.63	−0.42	−0.50	0.05	−0.12	−0.27	−0.10	1.75	1.74
CH_3	−0.60	−0.65	−0.19	−0.28	0.00	−0.11	−0.20	−0.11	1.69	1.75
F	−0.69	−0.71	0.25	0.17	−0.01	−0.13	−0.20	−0.11	1.68	1.75
Cl	−0.63	−0.64	−0.25	−0.32	−0.05	−0.16	−0.17	−0.09	1.67	1.74
Br	−0.60	−0.63	−0.33	−0.39	−0.03	−0.15	−0.19	−0.09	1.68	1.74
OH	−0.71	−0.73	0.15	0.07	−0.01	−0.12	−0.20	−0.12	1.71	1.75

[a] Endo and exo forms are given as shown.

Scheme 8

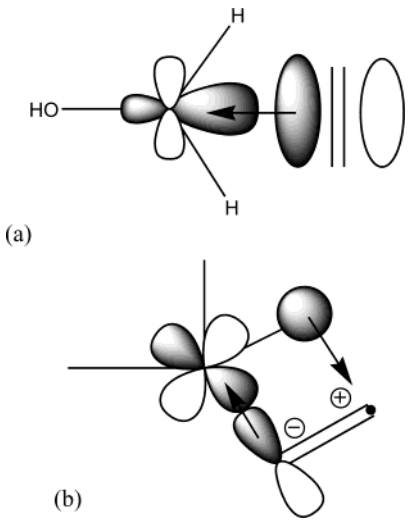

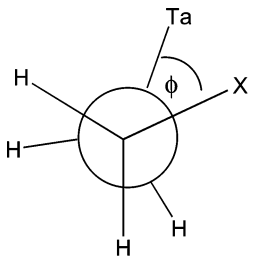

X	ϕ^o
F	1
Cl	42
Br	31
OH	22
OCH_3	17
H	2
CH_3	64

Figure 8. Newman projections about the $C_\alpha-C_\beta$ bond, with C_β to the front. ϕ indicates the angle of torsion away from eclipsed.

accompanying inductive effect is also seen; C_α develops a negative charge when the substituent is fluoride (−0.54) and less so for bromide and chloride (−0.45). This coincides with the barriers observed both by experiment and for the calculated exo insertion and, hence, supports the predominance of charge transfer effects in this insertion mode. The same arguments apply to the vinyl ether species, which have charge induction effects akin to that of fluoride, but with a HOMO/LUMO gap close to that of vinyl chloride. The HOMO/LUMO gap is greatest for H and CH_3 (179.2 and 174.5 kcal/mol, respectively), and there is very little charge asymmetry between C_α and C_β, hence providing a lower impetus for TS stabilization via the exo form, without affecting the enhanced ability for π-donation that predominates in the preferred endo insertion.

4. Alkyl Complex. B3LYP/LACVP* optimizations were performed for the insertion products, $Ta(CH_2-CH_2X)(H)(OH)_3$, with the hydride and alkyl (CH_2CH_2X) groups again oriented in the preferred equatorial plane. The crystal structure of $Ta(CH_2CH_2O^tBu)(H)(OSi^tBu_3)_3$ exhibits this same structural preference, although solution-phase and crystallographic experiments[7] suggest the presence of a more staggered than eclipsed conformation about the $C_\alpha-C_\beta$ bond. Computationally, a range of torsional angles close to eclipsed ($\phi < 30°$, except for Cl and CH_3, in which ϕ is closer to gauche) are observed, in each of which the X substituent is positioned close to the metal and is in the equatorial plane (see listing of angles and Newman projections in Figure 8). A study of conformers of $Ta(CH_2CH_2OCH_3)(H)(OH)_3$ revealed a near-eclipsed interaction between Ta and OCH_3 that leads to a significant energetic stabilization of 8.6 kcal/mol relative to the staggered conformation (optimizations starting with the gauche conformation converged to the eclipsed). When this value is added to the energetic preference for staggered 1-methoxypropane versus the eclipsed conformer (4.9 kcal/mol), an upper limit of −13.5 kcal/mol can be assigned to the Ta···OCH_3 interaction energy. The absence of experimental β-X elimination products for the X = O^tBu system suggests that the otherwise favorable metal−heteroatom interaction (such as that which causes the eclipsing in the OCH_3 model species assessed above) is interrupted by steric conflict between the siloxy ligand and the β-O^tBu group.

Significant β-X interactions are also observed in the Ta−X distances and in the C_β−X elongation. The agostic metal−β-H interaction characterized by Ziegler et al. for the Kaminsky-type catalysts (Cp_2Zr^+)[23] is observed here for the $Ta(CH_2CH_3)(H)(OH)_3$ complex. The net effect of this interaction is reduced somewhat, as a consequence of the lower electrophilicity of the noncationic tantalum center (d(M−β-H) = 2.059 Å for Cp_2ZrBu^+ and 2.509 Å for $Ta(Et)(H)(OH)_3$); d(C_β−β-H) = 1.184 Å for Cp_2ZrBu^+ and 1.116 Å for $Ta(Et)(H)(OH)_3$). Analogous electrostatic Ta−β-X interactions are observed for the halo- and alkoxy-substituted species. One can compare the C_β−X distances with those occurring in the analogous ethane derivatives, CH_3CH_2X, in which a considerable bond elongation is observed (Table 6). This bond elongation is most significant for C_β−F (4.7%) and least significant for C_β−Cl (1.8%), in the order Cl < Br < OH < H < F. For the case of X = CH_3, a slight bond shortening is actually observed. Note again the anomalous ordering of the halides with respect to group. The lesser elongation of the C_β−Cl distance can be related to the near-gauche conformation about the $C_\alpha-C_\beta$ bond, which leads to a reduced Ta−β-X interaction.

The Ta−X distances (2.4−3.3 Å) are noticeably shorter than the significant β-X interaction candidacy range prescribed by Cundari et al. (M−X ∈ [3.35−3.80 Å])[58] and approach the bonding limit for these systems

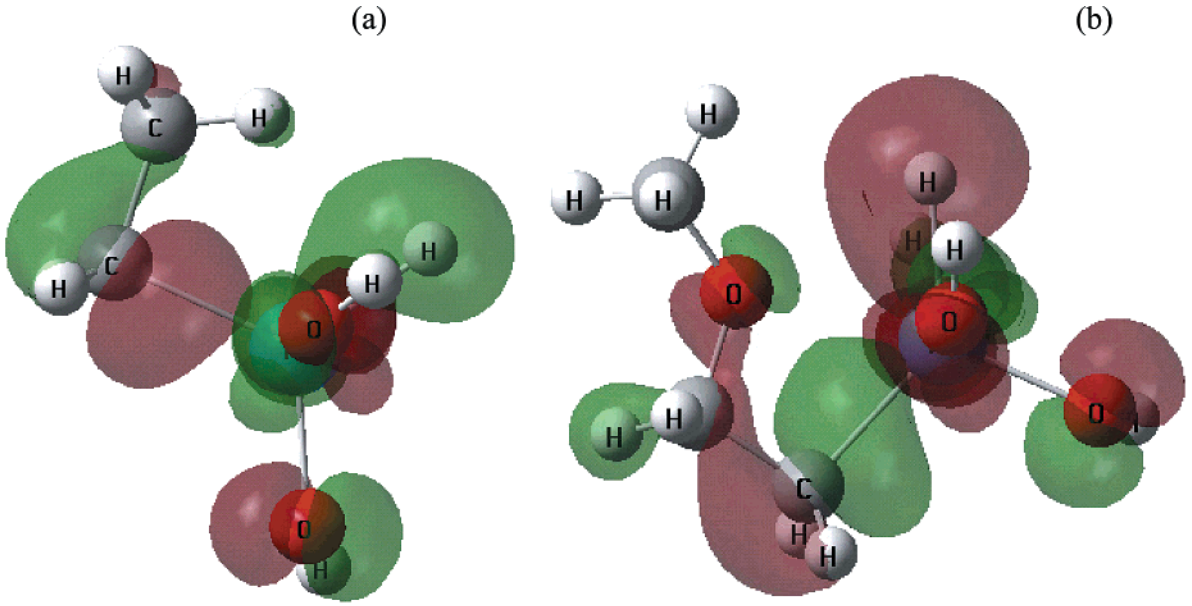

Figure 9. KS-HOMO for (a) $Ta(H)(CH_2CH_2OCH_3)(OH)_3$ and (b) $Ta(H)(CH_2CH_3)(OH)_3$.

Table 6. Comparison of C−X Bond Lengths (Å) in CH_3CH_2X (alkyl) and $Ta(CH_3CH_2X)(H)(OH)_3$ (complex), with Absolute and Percentage Differences (Δd(C,X) and % Δ, Respectively)

C−X	alkyl	complex	Δd(C,X)	% Δ
H	1.080	1.120	0.040	3.7
F	1.394	1.459	0.065	4.7
Cl	1.824	1.856	0.032	1.8
Br	1.988	2.035	0.047	2.4
OH	1.424	1.469	0.045	3.2
CH_3	1.55	1.536	−0.014	−0.9

(Ta−X ∈ [1.85−2.65Å], taken from a survey of Ta−X compounds in the CSD).

The lower Ta−C_α distances (2.15, 2.16 Å) in $Ta(H)(CH_2CH_2R)(OH)_3$ (R = H, CH_3, respectively, compared to 2.20−2.22 Å for the heteroatom-substituted alkyls) can be correlated with the diminished capacity for directed electronic interaction between the Ta and R groups. For the case of R = CH_3, the methyl hydrogens provide a steric barrier to such interactions, and the complex prefers a gauche orientation. In the R = H case (in which the eclipsed and gauche forms are essentially degenerate), it can be postulated that the lack of lone-pair contributions diminishes the capacity for substantial β-X interaction, compared to those available to main-group halogens and −OR. The diminution in Ta−X interaction is compensated by an increased Ta−C_α interaction, in a seesaw like effect in which the d_{xy} orbital of tantalum acts as a pivot.

This argument can be clarified from an orbital perspective. The KS-HOMO for $Ta(H)(CH_2CH_2OCH_3)(OH)_3$, as shown in Figure 9a, for example, manifests significant orbital interactions between the p character of the methoxy oxygen and the Ta−C bond. For the case of X = H (Figure 9b), the spherical symmetry of the s orbital leads to a less efficacious β-X interaction acting through the adjacent tantalum−hydride bond. A diminution is also noted for X = Cl, the gauche orientation of which prevents such close-neighbor interactions.

(58) Cundari, T. R.; Deng, J.; Pop, H. F.; Sarbu, C. *J. Chem. Inf. Comput. Sci.* **2000**, *40*, 1052−1061.

Chart 2

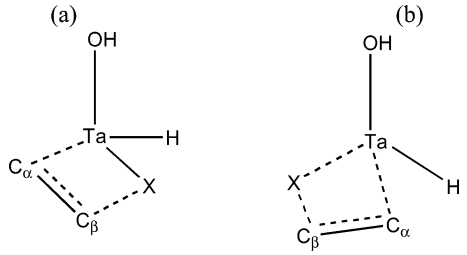

5. β-X Elimination Transition State. The Ta−β-X interactions culminate in an eventual β-X elimination reaction, which is very fast for the vinyl halides, somewhat slower for the vinyl ethers, and thermodynamically opposed for X = H, Me ($\Delta H^{\ddagger}_{elim}$ = 23.3 and 16.8 kcal/mol, respectively). As for insertion, there are two key modes for β-X elimination, namely exo (in which the olefin dissociates from the side; Chart 2a) and endo (in which the olefin dissociates between the X and the hydride; Chart 2b).

Enthalpic elimination barriers for exo β-X elimination decrease in the order CH_3 (50.0 kcal/mol) > H (33.3 kcal/mol) > OCH_3 (19.0 kcal/mol) > OH (17.7 kcal/mol) > F (7.3 kcal/mol) > Cl (6.5 kcal/mol) > Br (4.4 kcal/mol). The corresponding barriers for an *endo* β-X elimination are as follows: F (13.4 kcal/mol) > Cl (13.5 kcal/mol) > OH (56.9 kcal/mol) > OCH_3 (26.7 kcal/mol) > H (28.4 kcal/mol) > CH_3 (43.1 kcal/mol). These barriers indicate that elimination follows the same geometric preference as insertion, i.e., that the heteroatom X follows an exo pathway, and softer X species eliminate via the endo mechanism. The calculated enthalpic exo β-OCH_3 elimination barrier (19.0 kcal/mol) is closer to the free energy barrier determined by SW for $Ta(CH_2CH_2OCH3)(H)(OSi^tBu_3)_3$ (20.2 kcal/mol) than to the endo barrier (26.7 kcal/mol), providing further evidence for this preference.

Both exo and endo TS for β-X elimination are relatively early for all but the unusual exo TS for X = H discussed earlier. The exo TS is earlier for the vinyl halides than for the vinyl ethers. Wolczanski's geometric rationalization of the elimination kinetics (whereby the

Table 7. Change in Ta−X Distances (*d*, in Å) from the Alkyl Complex $Ta(CH_3CH_2X)(H)(OH)_3$ to the Product $Ta(H)(X)(OH)_3$, Given as Δ′[a]

X	*d*	Δ¢	$\Delta H^{\ddagger}$	X	*d*	Δ¢	$\Delta H^{\ddagger}$
F	0.625	0.96	7.3	OCH_3	0.492	0.95	19
Cl	0.968	0.74	6.5	H	0.741	1.34	28.4
Br	0.706	0.62	4.4	CH_3[b]	1.446		43.1
OH	0.485	0.95	17.7				

[a] Covalent estimates provided in ref 7 are given as Δ′. β-X elimination barriers (in kcal/mol) are given for comparison. [b] Covalent estimate for X = CH_3 not given in ref 7.

Chart 3

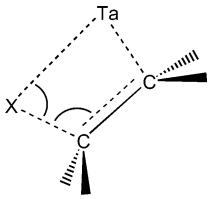

elimination barrier is correlated with the distance X must traverse before Ta−X formation) is incomplete. The calculated Ta−X distances between the alkyl complex and elimination TS predict an ordering of Br > F > Cl for the halides (Table 7). Nor does a simple electrostatics model suffice. Turning to the NBO characterization of the TS (Table 4b), one observes a multiplicity of bond cleavage and formation phenomena occurring to different extents among the eliminating species. A simple thermodynamic model can be proposed for the elimination enthalpy on the basis of these effects:

$$\Delta H = D(\mathrm{Ta{-}C}) + D(\mathrm{C{-}X}) - D(\mathrm{Ta{-}X}) - D(\mathrm{C{=}C})$$

where *D*(A−B) is the dissociation energy for the A−B bond.

The most obvious differentiating features that would contribute to a heightening of the elimination barrier of the three types of elimination species (halides, alkoxides, alkyls) are advancements of the endothermic C−X and Ta−C bond dissociations in the TS. The appropriate trends are indeed observed for the exo elimination, with bond orders indicating greater cleavage for the alkyl species (H, CH_3), followed by the alkoxides, and finally by the halides (Table 4b). C−X σ/σ^* energy gaps in the alkyl complex (calculated by NBO) are also highest for the alkoxides and fluoride (625−650 kcal/mol), followed closely by H and CH_3 (581−610 kcal/mol), and then decreasing rapidly down the halide group (Cl, 438 kcal/mol; Br, 337 kcal/mol). It should be clear that a lower energy gap implies a lower resistance to bond cleavage and, therefore, elimination itself. Offsetting these effects are π-bond formation, −*D*(C=C), and Ta−X formation, −*D*(Ta−X).

Endo elimination follows similar trends, with insertion barriers elevated by ∼8 kcal/mol for the halides and ethers and decreased by a similar amount for β-H and β-Me elimination (5 and 7 kcal/mol, respectively).

Geometrically, one observes a smaller elimination angle ($C_\alpha C_\beta X$) for the divalent alkoxides (106°), which indeed suggests a steric constraint to TS formation (Chart 3). Conversely, the more diffuse and univalent bromide leads to a more accessible elimination angle at C_β (111°). This argument leads to the correct conclusion that heavier halides (Br, Cl: 111°) eliminate faster than light halides (F: 105°), which are again faster than for the divalent alkoxides. For the case of X = CH_3, however, the reverse extreme is required; the elimination angles of $C_\alpha C_\beta X$ = 121° and $TaXC_\beta$ = 70.6° are indicators of the significant steric obstruction at the eliminating, hypervalent C_γ center.

Table 8. Thermodynamic Estimates $\Delta E_h'$ Made Relative to β-H Elimination, through the Sum of Relative C−X Bond Dissociation Energies, $D(C{-}X)_h$, with Relative Ta−X Bond Formation Energies, $-D(Ta{-}X)_h$[a]

X	$D(C{-}X)_h$	$D(Ta{-}X)_h$	$\Delta E_h'$	ΔE_h	ϵ
F	+0.17	73.2	−73.0	−51.3	21.7
Cl	−28.7	25.6	−54.3	−41.1	13.3
Br	−36.7	25.8	−62.5	−43.0	19.4
OH	−18.5	43.1	−61.6	−39.3	22.3
H	0.0	0.0	0.0	0.0	0.0
CH_3	−19.1	−10.0	−9.1	−6.6	2.5

[a] Actual relative elimination energies, ΔE_h, and the difference, $\epsilon = \Delta E_h - \Delta E_h'$, are also given. All values are given in kcal/mol.

6. Elimination Thermodynamics. The calculated elimination enthalpies are exothermic for the halide and alkoxy species (F (−28.0 kcal/mol) > Br (−19.7 kcal/mol) > Cl (−17.7 kcal/mol) > OH (−15.9 kcal/mol) > OCH_3 (−13.8 kcal/mol), in order of exothermicity) and endothermic for the hydride and methyl species (H (23.3 kcal/mol) > Me (16.8 kcal/mol), in order of endothermicity). When the thermodynamics are expressed as above, the various terms leading to the energy of elimination can be evaluated. If it is assumed that the *D*(Ta−C) and *D*(C=C) contributions are the same for each of the eliminating species, then the variation in enthalpies of elimination can be attributed to a coupling of *D*(Ta−X) and *D*(C−X).

D(Ta−X) can be estimated relative to Ta−H by means of the equation

$$Ta(H)(X)(OH)_3 + H^{\bullet} \rightarrow Ta(H)_2(OH)_3 + X^{\bullet}$$

The B3LYP/LACVP* values for $D(Ta{-}X)_h$, where $D(Ta{-}X)_h = D(Ta{-}X) - D(Ta{-}H)$, are +73.2 kcal/mol (F), +25.6 kcal/mol (Cl), +25.8 kcal/mol (Br), +43.1 kcal/mol (OH), 0.0 kcal/mol (H), and −10.0 kcal/mol (CH_3) (Table 8).

$D(C{-}X)_h$ can be determined similarly:

$$CH_3X + H^{\bullet} \rightarrow CH_4 + X^{\bullet}$$

yielding $D(C{-}F)_h$ = 0.17 kcal/mol, $D(C{-}Cl)_h$ = −28.7 kcal/mol, $D(C{-}Br)_h$ = −36.7 kcal/mol, $D(C{-}OH)_h$ = −18.5 kcal/mol, and $D(C{-}CH_3)_h$ = −19.1 kcal/mol. Combining these two effects, $D(C{-}X)_h - D(Ta{-}X)_h$, one can approximate the enthalpies of elimination relative to β-H elimination, yielding the ascending endothermicities F > Br > OH > Cl ≫ CH_3 > H (Table 8). While this correctly predicts β-F elimination to be the most exothermic and β-H elimination to be the most endothermic, it fails to account for the lower exothermicity of β-OH elimination relative to the β-Cl elimination. This may be a result of variation in the assumed constant π-bond formation energies occurring in elimination (implying that the C−C σ bond energy is quite dependent on the substituent X) and the neglect of stabilizing Ta−β-X interactions in the precursor alkyl

complex. By the method of subtraction (subtracting the approximated $D(C-X)_h$ and $-D(Ta-X)_h$ relative terms from the relative elimination energies determined from the reaction profile) one sees that these effects are not insubstantial (on the order of 0−20 kcal/mol) and are more significant for the ethers and fluoride, decreasing to bromide and then chloride and finally X = CH_3.

Summary and Conclusions

Olefin insertion and β-X elimination reaction coordinates about a pentacoordinate tantalum(V) complex, $Ta(H)_2(OH)_3$, have been studied using density functional theory and effective core potentials (B3LYP/LACVP*). Computational characterization of the complex indicates a bis-equatorial arrangement of the hydrides about the trigonal-pyramidal tantalum coordination sphere, providing calculated vibrational modes that agree with the reported infrared frequencies for the related complex $Ta(H)_2(OSi^tBu_3)_3$. Other evidence (molecular orbital theory and the nature of other pentacoordinate tantalum complexes, including those modeled in this work) for a bis-equatorial-hydride assignment also counters the previous assignment of bis-axial-hydride geometry to the $Ta(H)_2(OSi^tBu_3)_3$ species.[45]

Lower insertion barriers are observed for the vinyl ethers (for which elimination is rate limiting), followed by the vinyl halides in the order F < Br < Cl. In addition to this, it is also found that both of these Lewis base substituted groups insert via an exo approach to the tantalum dihydride. The hydrocarbon alkenes, such as ethylene and propylene, however, preferentially insert via an endo approach, which has insertion barriers akin to those of the vinyl halides (∼5−7 kcal/mol). No evidence was found for an olefin-bound complex preceding insertion, in accord with the low insertion barriers observed.

Electronic structure analysis of the insertion process emphasizes the interaction of π/π^* frontier orbitals on the olefin with the HOMO and nonbonding LUMO of the tantalum hydride complex, a Bercaw charge-transfer nature being the case for the exo mode and a standard Hoffmann donor/acceptor insertion for the endo.

A similar result is observed for the elimination process, in which significant Ta−X interactions in the intermediate alkyl complex can lead to Ta−X bond formation and the elimination of ethylene from the complex. This process is exothermic for the ethers and halides and endothermic for the elimination of hydride and methyl species, a consequence of the strongly preferential Ta−O/X binding (a hard/hard interaction) as opposed to Ta−H/C (hard/soft). Correspondingly, one finds higher barriers for the elimination of hydride and methyl than for the halides and ethers, for which a lower elimination barrier is presented for the halides than the ethers, in order of size (i.e., Br eliminates more quickly than Cl, which is faster than F). Elimination barriers for the vinyl halides are found to be of the same order as for insertion (experiment indicates that they should be much lower), a fact that may be a consequence of the steric disparity between computational and experimental systems. Further calculations using larger model systems could serve to verify the accuracy of the computational model proposed, as well as providing an extended data set from which one can consider the olefin insertion and β-X elimination procedures from a more generalized standpoint.

Scheme 9

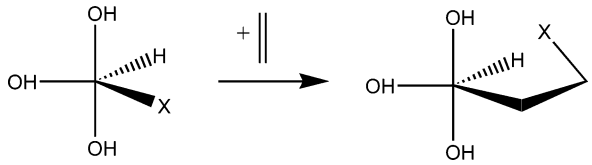

Relevance to Ziegler−Natta Polymerization. The nature of this research also makes it convenient for comment upon the relationship between β-X elimination and the polymerization of functionalized olefins. Chain propagation barriers for ethylene can be estimated at 26.3 kcal/mol from the reverse barrier for endo β-CH_3 elimination. For heteroatom-substituted olefins an exo propagation step seems likely, with an approximate chain propagation barrier of ∼33 ±10 kcal/mol to account for variations in substituent X. When these values are compared to the β-X elimination barriers (4.4−19.0 kcal/mol), it can be readily seen that β-X elimination will doubtless occur at a faster rate than chain propagation, even without the inclusion of similarly unfavorable entropic factors involved in the association of olefin and catalyst.

Also of interest is the insertion of an olefin into the elimination product, $Ta(H)(X)(OH)_3$ (Scheme 9). If this reaction is favorable, then β-X elimination would no longer be a terminal process but, rather, one which generates a new, alternative catalyst species. The reverse elimination barriers, however, are high (24−41 kcal/mol), and the intermediate alkyl complex is thermodynamically unstable. Thus, β-X elimination does indeed bode poorly for catalyst poisoning in these systems.

Current approaches to overcoming β-X elimination for the synthesis of functionalized polymers involve indirect methods such as postmodification,[59] spacing of the functionality away from the olefin double bond,[60] and adoption of free-radical procedures.[61] Each of these methods involve additional cost, compromises on the polymer microstructure, or extreme synthetic conditions. The generation of a catalyst suitable for the direct polymerization of functionalized olefins would therefore be of great industrial and scientific interest. As the results of this research suggest, β-X elimination poses the major hurdle to such a task, and therefore the generation of such a catalyst involves the taming of this catalyst-degrading event.

Since β-X elimination proceeds most rapidly via the exo mechanism, it is reasonable to suggest that blocking the exo pathway will inhibit β-X elimination. This would raise the elimination barriers from a range of 4−20 kcal/mol to a range of 15−50 kcal/mol, as the endo mechanism becomes preferable. The latter range is closer to the order of chain propagation (estimated above at 33 ± 10 kcal/mol), and thus polymerization may become feasible for some systems. Inhibition of the exo mech-

(59) Chung, T. C. *CHEMTECH* **1991**, *21*, 496−499.
(60) Boffa, L. S.; Novak, B. M. *Chem. Rev.* **2000**, *100*, 1479−1496.
(61) Claver, G. C.; Cotman, J. D., Jr.; Gonzalez, M. F. *J. Polym. Sci.* **1967**, *5*, 1137−1164.

Scheme 10

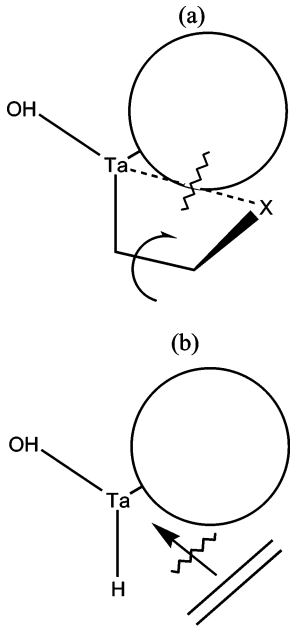

anism may be achieved by replacing the spectator hydride with a bulkier alkyl ligand, for example. This would also have the effect of inhibiting the endo insertion pathway. The insertion of non-heteroatom-substituted olefins, such as ethylene and propylene, would therefore be disfavored, with a lesser effect on exo inserting olefins (such as the vinyl halides and ethers). These points are illustrated in Scheme 10.

Further modeling and analysis of the electronics of the β-X elimination process may suggest ways in which the electronic environment of the complex may be altered so as to diminish the M−β-X interactions or, possibly, to even utilize them for assisting subsequent olefin insertions. This latter conjecture is readily conceivable in that the subtle β-X interactions in the alkyl complex alter the geometry of the resting state and the electronics of the metal center, thereby presenting a different face to olefin insertion as in the dihydride complex, for example. Substitution by another metal and ligand modification are two prospective procedures via which electronic control can be made, both of which are amenable to further computational development and exploration.

Acknowledgment. We thank the National Science Foundation for support of this research through Grant No. CHE-9983665. Additionally, C.D.T. acknowledges the support of the University of Memphis and the University of Western Australia for fellowship support through the Van Vleet and Hackett foundations. Helpful discussions with Prof. Peter T. Wolczanski (Chemistry, Cornell University) are also acknowledged.

Supporting Information Available: Tables giving Cartesian coordinates for B3LYP/LACVP* optimized geometries. This material is available free of charge via the Internet at http://pubs.acs.org.

OM0303606